Effect of solar simulated N-doped TiO$_2$ photocatalysis on the inactivation and antibiotic resistance of an *E. coli* strain in biologically treated urban wastewater

L. Rizzo [a,*], D. Sannino [b,**], V. Vaiano [b], O. Sacco [b], A. Scarpa [a], D. Pietrogiacomi [c]

[a] *Department of Civil Engineering, University of Salerno, via Giovanni Paolo II, 1-84084 Fisciano, SA, Italy*
[b] *Department of Industial Engineering, University of Salerno, via Giovanni Paolo II, 84084 Fisciano, SA, Italy*
[c] *Department of Chemistry, University "la Sapienza" of Rome, piazzale Aldo Moro 5, 00185 Roma, Italy*

A B S T R A C T

The effect of N-doped TiO$_2$ (NDT) photocatalysis on the inactivation of an antibiotic resistant *Escherichia coli* strain selected from a biologically treated urban wastewater effluent was investigated. NDT was prepared by sol–gel method and characterized by thermogravimetric analysis, X-ray diffraction, FTIR and Laser Raman spectra and UV–visible reflectance spectra. XRD analysis revealed that anatase is the only crystalline phase in NDT photocatalyst and UV–visible reflectance spectra showed that the absorption onset shifted toward visible region (about 500 nm). The NDT photocatalyst was compared with commercially available TiO$_2$ powders (namely Millennium PC50 and PC100), under solar simulated radiation (250 W lamp) and different photocatalysts loadings (0.025–0.5 g L^{-1}). The higher inactivation rate (8.5×10^5 CFU 100 mL^{-1} min^{-1}, after 10 min of irradiation) of antibiotic resistant *E. coli* strain was observed for NDT photocatalyst at 0.2 g L^{-1} dose. Kinetic test at the optimum photocatalyst loading showed that total inactivation can be achieved after 60 min of irradiation. Antibiotic resistant test (Kirby–Bauer) on survived colonies showed that solar photocatalytic process with NDT did not significantly affect resistance of *E. coli* strain to tetracycline and vancomycin as irradiation time increased, but a decreasing trend ($p < \alpha = 0.05$) in resistance to ciprofloxacin ($p = 0.0311$) and sensitivity to cefuroxime ($p = 0.0018$) was observed.

1. Introduction

The extensive use of antibiotics (for human, veterinary and aquaculture purposes) has led to their continuous release into the environment and possible development of antibiotic resistance in bacterial populations, which make antibiotics ineffective in the treatment of microbial infections [1]. Conventional urban wastewater treatment plants (UWWTPs), typically based on biological processes, are among the main hotspots of antibiotics [2] and antibiotic resistant bacteria (ARB) [3] spread into the environment. The release of ARB from UWWTPs effluents into receiving surface waters may be due to either: (i) absence of disinfection process (in some Countries effluent from UWWTPs are disposed off without any disinfection) or (ii) inadequacy of conventional disinfection processes (e.g., chlorination and UV radiation) to effectively inactivate ARB [4].

Accordingly, alternative disinfection techniques, such as advanced oxidation processes (AOPs), should be investigated in order to evaluate their efficiency in removing ARB from domestic effluents. AOPs include different processes (e.g., Fenton, photo-Fenton, TiO$_2$ photocatalysis, UV/O$_3$, UV/H$_2$O$_2$, etc.) and are based on the in situ generation of powerful transitory species, principally the hydroxyl radical (HO$^\bullet$) which can oxidize a wide range of organic contaminants [5–7]. In spite of the disinfection efficiency of AOPs has been widely investigated [8,9] there is a lack of studies on their effect on purposely selected ARB [3]. Among AOPs, TiO$_2$ photocatalysis has recently emerged as interesting water disinfection option, because: (i) it does not result in the formation of toxic disinfection by-products compared to chemical disinfectants [10–12] and (ii) it can be operated under solar radiation thus lowering the operation cost considerably [13]. However, due to TiO$_2$ capacity to absorb only about 4% of the solar irradiation, different approaches to broad the absorption of TiO$_2$ toward the visible region have been developed to improve the photocatalytic treatment efficiency. These approaches include either anchoring of organic or inorganic dyes on the TiO$_2$ surface or doping by: (i) metal ions [14], (ii) non-metallic species such as N and S [15–17], (iii) introducing oxygen vacancies that

* Corresponding author. Tel.: +39 089 969334; fax: +39 089 969620.
** Corresponding author. Tel: +39 089 964092; fax: +39 089 964057.
E-mail addresses: l.rizzo@unisa.it (L. Rizzo), dsannino@unisa.it (D. Sannino).

generate color centers reducing TiO_2 band-gap [18]. Nitrogen, carbon and sulfur doping of TiO_2 have been carried out by several ways, such as co-precipitation, solvothermal, sol–gel, microemulsion, electrochemical, chemical or physical vapor deposition and ion-implantation methods, but also by solid–solid reaction. However the sol–gel technique resulted in more homogeneous product, yielding high purity and controlled stoichiometry, being easy to regulate the dopant introduction and the final composition [19].

In particular, in sol–gel synthesis of N-doped photocatalyst, several titania and nitrogen precursors have been employed, such as $TiCl_4$ or titanium tetra-isopropoxide (TTIP) and urea or ammine. However only few studies reported the optimization of sol–gel preparation of these photocatalysts [6]. In this work, an optimized N-doped TiO_2 (NDT) photocatalyst was synthesized to evaluate the improved capacity, compared to commercially available TiO_2 photocatalysts (namely Millennium PC50 and PC100), in photocatalytic disinfection of biologically treated urban wastewater inoculated with an antibiotic resistant *Escherichia coli* strain. Commercially available TiO_2 photocatalysts Millennium PC50 and PC100 were selected for comparative tests because they have characteristics similar to NDT photocatalyst synthesized in this work. The NDT photocatalyst was characterized by thermogravimetric analysis (TG-DTG), X-ray diffraction (XRD), Laser Raman spectra, Fourier transform infrared spectroscopy (FTIR) and UV–visible reflectance spectra, particles size analysis. Specific surface area and point of zero charge (PZC) of the NDT photocatalyst were also measured. The photocatalytic inactivation of the selected antibiotic resistant *E. coli* strain was evaluated under solar simulated radiation (250 W lamp) and different photocatalysts loadings (0.025–0.5 g L^{-1}). Antibiotic resistance to ciprofloxacin (CIP), cefuroxime (CEF), tetracycline (TET) and vancomycin (VAN), prior to and after the photocatalytic treatment, was evaluated by Kirby–Bauer method.

2. Materials and methods

2.1. Materials

Anatase titania samples (PC50 and PC100) were provided by Millennium Inorganic Chemicals. Ammonia aqueous solution at 30 wt% and 97 wt% titanium tetraisopropoxide were purchased from Carlo Erba and Sigma Aldrich, respectively.

2.2. N-doped TiO_2 preparation

NDT photocatalyst was prepared by the sol–gel method, according to the method reported in [6,20]. A volume of 100 mL ammonia aqueous solution at 30 wt% was added drop wise to 25 mL of 97 wt% titanium tetraisopropoxide at 0 °C while the solution was vigorously stirred, leading to the formation of a white precipitate. The precipitate was carefully washed with demineralised water and centrifuged to be separated. Finally, the obtained powders were dried and calcined at 450 °C at different times (10, 20, 30 and 40 min) to get an optimized visible photoactive TiO_2. The obtained samples were yellow in color.

For comparison, undoped TiO_2 was prepared with the same method but adding 100 mL of demineralized water (without ammonia) to 25 mL of 97 wt% titanium tetraisopropoxide.

2.3. Catalyst characterization

The catalysts were characterized by several techniques. UV–vis reflectance spectra (UV–vis DRS) of catalysts were recorded by a PerkinElmer spectrometer Lambda 35 using a RSA-PE-20 reflectance spectroscopy accessory (Labsphere Inc., North Sutton, NH). All spectra were obtained using an 88 sample positioning holder, giving total reflectance relative to a calibrated standard SRS-010-99 (Labsphere Inc., North Sutton, NH).

The reflectance data were reported as the $F(R_\infty)$ value from Kubelka–Munk theory vs the wavelength. Band gap determinations were made by plotting $[F(R_\infty) \times h\nu]^2$ vs $h\nu$ (eV) and calculating the x intercept of a line passing through $0.5 < F(R_\infty) < 0.8$. Thermogravimetric analysis (TG-DTG) of samples was carried out in air flow with a thermo balance (SDT Q600, TA Instruments) in the range 20–1000 °C at 10 °C min^{-1} heating rate. Samples were analyzed without pretreatment, with a fast start of temperature program, to avoid dehydration in the anhydrous air stream.

Specific surface area (BET) was evaluated from dynamic N_2 adsorption measurement at −196 °C, performed by a Costech Sorptometer 1040 after pretreatment at 120 °C for 30 min in He flow.

Mass titration method was used to estimate the acidity of sample powders useful to measure the PZC of the photocatalysts investigated in this work. The mass titration experiments were performed using procedures described elsewhere [21]. Shorter stabilization times after each powder addition (2 h in this study) were used to minimize possible dissolution of sample powders.

X-ray diffraction (XRD) measurements were carried out using an X-ray micro diffractometer Rigaku D-max-RAPID, using Cu-Kα radiation.

Laser Raman spectra were obtained at room temperature with a Dispersive MicroRaman (Invia, Renishaw), equipped with 785 nm diode-laser, in the range 100–2500 cm^{-1} Raman shift.

FTIR measurements were carried out by a spectrometer (PerkinElmer 2000), equipped with a MCT detector, operating at a resolution of 4 cm^{-1}. The powdered samples were pelletted (pressure, 2×10^4 kg cm^{-2}) in self-supporting disks of ca. 10 mg cm^{-2}, and put in an IR cell that allowed heating in presence of helium atmosphere.

Particle size (PS) and particle size distribution (PSD) were measured by dynamic laser scattering (DLS) using a Nanosizer (NanoZS Malvern Instrument, UK) equipped with a He–Ne laser operating at 5.0 mW and 633 nm that measures the hydrodynamic diameter of the particles. Photocatalysts were dispersed in distilled water. DLS analysis was performed setting temperature at 25 °C.

2.4. Wastewater sample

Wastewater samples were taken from a large UWWTP (250,000 equivalent inhabitants) located in southern Italy, in the effluent of the biological process (activated sludge), just upstream of the disinfection unit (chlorination). Samples were collected in sterilized 1 L amber glass bottles. The wastewater samples were analyzed before use for a number of qualitative characteristics:: pH 7.9, BOD_5 10.0 mg L^{-1}, COD 23.3 mg L^{-1}, TSS 32.5 mg L^{-1}, redox potential 63.6 mV, conductivity 1105 μS cm^{-1}.

2.5. Inoculum and sample preparation

Multi drug resistant *E. coli* strain was selected according to the procedure published in our previous work [22] and inoculated to autoclaved (15 min at 121 °C) wastewater samples. The selected *E. coli* strain was unfrozen and transferred in 10 mL physiological solution to achieve 10^7 CFU 100 mL^{-1} (0.5 McFarland). The physiological solution was finally added to 500 mL wastewater sample.

2.6. Photocatalytic tests

Photocatalytic experiments were carried out in 2.2 L cylindrical glass batch reactor (13.0 cm in diameter) filled in with 500 mL wastewater sample (5.0 cm water height). The reactor was placed in a water bath to maintain the temperature constant (roughly 30 °C) during the experimental procedure. The wastewater solution was

continuously stirred in the reactor. Solar irradiation was provided by a wide spectrum 250 W lamp equipped with a UV filter (Procomat, Italy), fixed at 40 cm from the upper water level in the reactor. A spectrometer model HR-2000 from Ocean Optics (Florida, USA), equipped with cosine corrector with Spectralon diffusing material, was used to measure irradiance spectra of UV lamp.

An appropriate amount of TiO_2 powder was added to the autoclaved wastewater sample and sonicated for 5 min. Then the inoculum was added in the solution. The effect of the photocatalyst loading on *E. coli* strain was investigated in the range 0.025–0.5 g L^{-1} for 10 min irradiation time. Control tests without any photocatalyst addition were also performed. As the photocatalyst dose was optimized, the inactivation kinetic (60 min total irradiation time) was determined.

2.7. Bacterial count

Bacterial count was performed by spread plate method. Briefly, small amounts of wastewater samples were diluted according to the expected number of colonies, 100 μL were spread on TBX agar medium (Sigma–Aldrich) and incubated at 44 °C for 24 h. Measurements were carried out in triplicates and average values and standard deviation were plotted as CFU 100 mL^{-1}.

2.8. Antibiotic resistance assay

Antibiotic resistance prevalence of bacterial colonies prior to and after the photocatalytic treatment was tested by Kirby–Bauer method. Briefly, the colonies survived to photocatalytic treatment and growth on TBX agar medium were collected from (4–5 colonies randomly selected from each one agar/irradiation time) and transferred in 10 mL physiological solutions, respectively, to achieve 10^7 CFU 100 mL^{-1} (0.5 McFarland). Then, bacterial suspensions were spread on Mueller Hinton agar (Biolife, Italy) using a sterile cotton swab. Antibiotic discs of CIP (5 mg), CEF (30 mg), TET (30 mg) and VAN (30 mg) (all from Biolife) were placed on the surface of each inoculated plate. After 24 h of incubation at 37 °C, the diameters of antibiotic inhibition of growth were measured. The procedure was duplicated and the average values plotted.

3. Results and discussion

3.1. Catalyst characterization

3.1.1. UV–visible spectra

UV–vis DRS spectra in terms of $F(R_\infty)$ of NDT can be decomposed into four peaks centered at about 250, 300, 350 and 410 nm respectively. The integration of the signal as a function of the wavelength of the fourth contribution is correlated to the amount of energy absorbed in the visible region. The latter is reported in Fig. 1 for different calcination times.

The amount of energy reached the highest value for a calcination time of 30 min.

The band-gap energy for NDT decreased as calcination time was increased up to 30 min (Fig. 2a). For a calcination time higher than 30 min, the value of band-gap energy increased.

These results demonstrate the ability of photocatalysts to absorb visible light due to the electronic transition. This typical absorption is due to the electronic transition from the isolated N 2p level, which is formed by incorporation of nitrogen atoms into the TiO_2 lattice, to the conduction band [23]. For this reason the catalyst NDT calcined for 30 min was chosen for the disinfection photocatalytic tests.

Stability of NDT photocatalyst was assessed by recycling experiments using different operating conditions and the results were
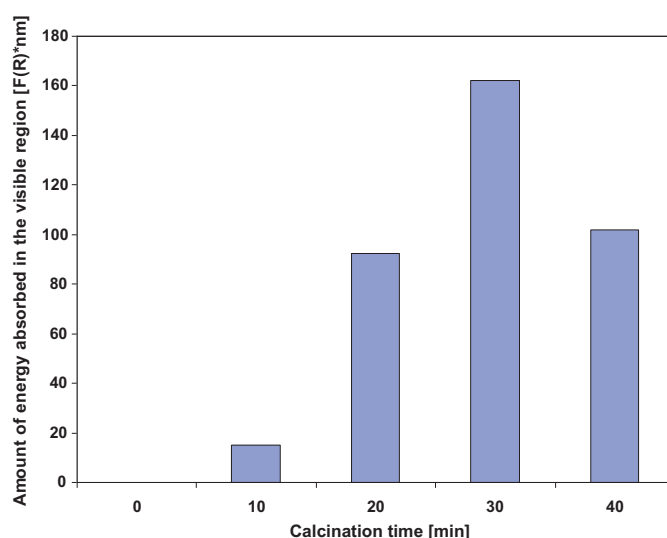

Fig. 1. Amount of energy absorbed in visible region by NDT catalyst as a function of calcination time.

published in our previous work [6]. Methylene blue (MB), a common organic dye frequently used to assess the photocatalytic activity, was used to evaluate stability. The amount of MB adsorbed under dark conditions on the recycled catalyst (32% after 120 min, initial MB concentration: 7.5 mg L^{-1}; incident light intensity: 32 mW cm^{-2}; catalyst dosage: 3 g L^{-1}) was lower than that one obtained with fresh catalyst (65% after 120 min). In spite of this, when the visible lamp was switched on, the photocatalytic activity remained high for the recycled catalyst too, because final MB removal (85% after 120 min irradiation) was as high as for the fresh catalyst, indicating that no deactivation took place.

In Fig. 3 the comparison of UV–visible reflectance spectra of PC50, PC100 and NDT nanoparticles are reported. The reflectance measurements on PC50 and PC100 showed that the absorption onset of these samples was 380 nm while the spectrum of NDT nanoparticles showed that the absorption onset shifted from 380 to about 500 nm. This range of wavelength implies that the activation energy can be provided by the energy related to the wavelength emission of the used lamp also in visible region for NDT photocatalyst as shown in Fig. 3.

PC50 and PC100 are activated with photons of energy of a longitude close to about 380 nm which involves a band gap in the range 3.3–3.4 eV, typical value for TiO_2 in anatase phase [24,25]. For the synthesized NDT, the doping process determined a decrease of band-gap value from 3.3–3.4 eV to 2.5 eV (Table 1).

These differences in the absorption property are markedly evidenced by plotting $[F(R_\infty) \times h\nu]^2$ vs $h\nu$ (Fig. 2b).

3.1.2. Specific surface area measurements

Table 2 reports the specific surface area of three samples evaluated by BET method. The commercial titania PC100 and PC50 sample showed values of 87 and 50 m^2 g^{-1}, respectively. The specific surface area of NDT photocatalyst was found to be similar to

Table 1
Crystallite size, PZC and band gap energy of PC50, PC100 and NDT photocatalysts.

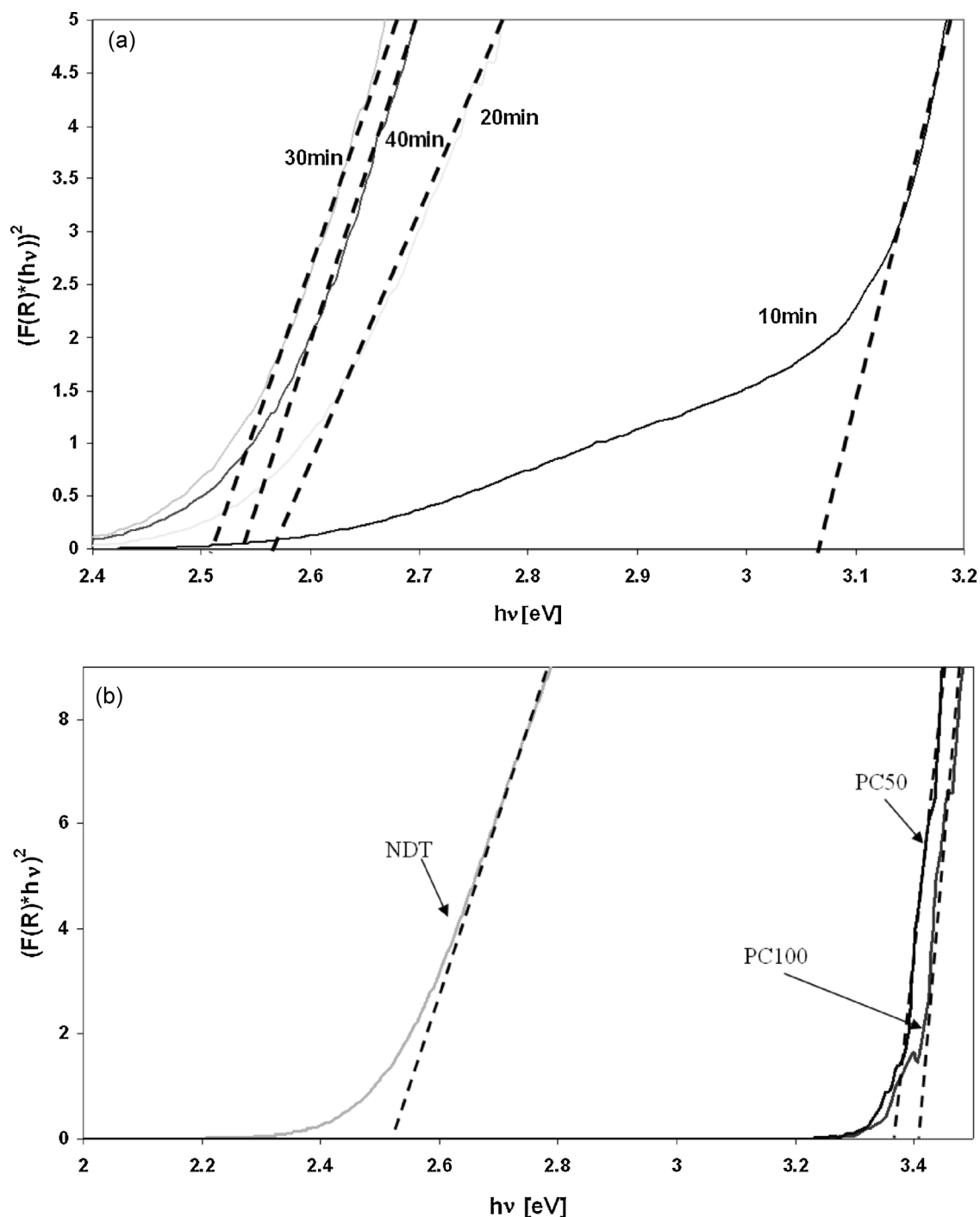| Catalysts	Crystallite size (1 0 1) (nm)	Crystallite size (2 0 0) (nm)	Crystallite size (2 0 4) (nm)	PZC (pH)	Band gap energy (eV)
PC50	17	9	17	4.0	3.3
PC100	16	17	11	3.1	3.4
NDT	17	14	9	7.6	2.5

Fig. 2. Band gap determination for NDT catalyst as a function of calcination time (a) and band gap calculation by UV–vis DRS spectra for PC50, PC100 and NDT photocatalyst calcined for 30 min (b).

PC100, confirming the right selection of the latter sample to be adopted as comparison for sol–gel N-titania, at parity of exposed surface. PC50 instead permits to evaluate the effects related to the surface by comparing with PC100 titania.

Table 2
SSA (BET), sulfate and hydroxyls density for PC50, PC100 and NDT photocatalysts.

Catalysts	BET ($m^2 g^{-1}$)	SO_4^{2-} surface density ($\mu mol/m^2$)	Hydroxyls density ($\mu mol/m^2$)
PC50	50	1.03	14.6
PC100	87	2.13	9.26
NDT	80	–	7.00

3.1.3. Termogravimetric analyses

Thermogravimetric results of NDT, PC50 and PC100 photocatalysts samples are shown in Fig. 4. For all the samples, a first main weight loss takes place below 180 °C, associated with hydration water desorption. The second step (present as a shoulder) that occurred up to about 390 °C, is related to the removal of OH⁻ surface groups of titania [26].

On NDT sample (Fig. 4c), the weight loss starting at about 380 °C could be due to the oxidation reaction of NH_3 or NH_2 which are bonded coordinately onto Lewis acid site with the oxygen released from amorphous grain-boundaries by forming oxygen deficient sites [27]. The amount of this loss is 0.16 wt%.
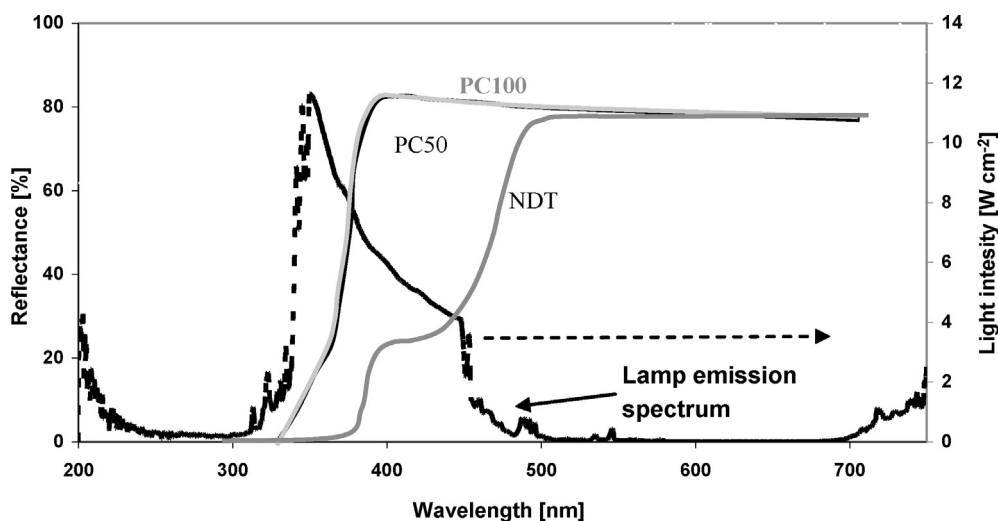
Fig. 3. Comparison between UV–vis spectra of PC50, PC100 and NDT photocatalysts and emission spectrum of lamp.

The last weight loss, present only for PC50 and PC100 catalysts, located at temperature higher than 600 °C, is attributed to the decomposition of sulfate species giving rise to gaseous SO_3 [26]. The hydroxyl groups and surface sulfates (as SO_4^{2-}) density evaluated in the range 180–350 °C and 400–800 °C respectively are presented in Table 2. As expected, the surface sulfate density increased by increasing the sulfate loading.

3.1.4. Raman spectra

Raman spectra of the three photocatalysts are reported in Fig. 5.

Among the three natural phases including rutile and brookite, anatase phase is retained to be the more active in photocatalysis. Anatase has tetragonal structure of space group D_{4h}^{19} with two formulas per unit cell and thus has six Raman active modes ($A1_g + 2B_{1g} + 3E_g$). In fact, the Raman modes at 141, 194, 394, 515 and 636 cm^{-1} are all assigned to the anatase phase and, correspondingly, could be assigned to E_g, E_g, B_{1g}, A_{1g} (or B_{1g}) and E_g modes in anatase phase, respectively. Bands related to nitrogen species on NDT are not detectable. For NDT photocatalyst the signal from 141 cm^{-1} moves to 144 cm^{-1}. It has been reported that the blue shift is related to changes of the oxygen stoichiometry instead of any internal stress or grain size effects [28]. The defect in oxygen stoichiometry may be due to the presence of nitrogen. The signal at 986 cm^{-1} is related to symmetric stretching mode ν_1 of sulfate, while the signals at about 1012 and 1018 cm^{-1} due to the S=O bonds of isolated sulfates [29] were not observed on PC50 and PC100 due to the low content of sulfate.

3.1.5. XRD measurements

XRD analysis confirmed anatase as the only one crystalline phase for PC50, PC100, while NDT exhibited strong diffraction peaks at 25° and 48° indicating that TiO$_2$ is mainly in anatase phase (Fig. 6). However, a broad and weak diffraction peak at 27° could indicate that only a minor fraction of TiO$_2$ is rutile [29].

The averaged anatase grain sizes were determined according to the Scherrer's equation $D = k\lambda/\beta \cos\theta$, where D is the grain size; k is a constant (shape factor, about 0.9); λ is the X-ray wavelength; β is the full width at half maximum of the diffraction line and θ is the diffraction angle corresponding to (1 0 1), (2 0 0) and (2 0 4) diffraction planes. The crystallites size values are reported in Table 1.

The TiO$_2$ crystallites size with reference to the (1 0 1) (2 0 0) and (2 0 4) diffraction planes was in the range of 9–16, 11–17 and 9–17 nm for PC50, PC100 and NDT, respectively. The three catalysts showed a very similar value with respect to (1 0 1) plane (between

16 and 17 nm), without relevant changes associated with the addition of nitrogen. Instead, TiO$_2$ crystallites size at (2 0 0) diffraction plane was 9, 17 and 14 nm and this value was 17, 11 and 9 nm at (2 0 4) diffraction plane for PC50, PC100 and NDT, respectively. This difference is due to the non pseudo-spherical shape of TiO$_2$ nanoparticles, and likely attributed to the faceted bipyramidal habitus [30].

3.1.6. Point of zero charge (PZC)

Mass titration method was used to estimate the acidity of sample powders. The PZC, which describes the acidity of oxide materials, may be measured using potentiometric titration, mass titration, or measurement of the wetting angles. The mass titration method of PZC characterization was initially proposed by Noh and Schwarz [21]. In this work, the mass titration studies were performed using procedures described elsewhere [21]. Shorter stabilization times after each powder addition (2 h in this study) were used to minimize possible dissolution of sample powders.

According to the method used, the trend of pH as a function of photocatalyst powder addiction is plotted in Fig. 7.

The final pH value was assumed as representative of PZC and it is reported in Table 1. In particular, the value of PZC of NDT is 7.6, more basic with respect to the values of PZC of 6.2 reported in literature for pure anatase titania [31], according to its amphoteric character. This basic character can be ascribed to the presence of surface nitrogen groups in the doped titania whose nature could be supposed to be an NH specie [32]. For the commercial PC50, the presence of sulfate increased surface acidity, leading to PZC value of 4, a stronger acid than that related to pure anatase phase. Accordingly, the increase in the surface sulfate load in PC100, as deduced by termogravimetric losses (Table 2), decreases PZC to 3.1 (Table 1).

3.1.7. FTIR

The FTIR spectra analysis of NDT (a) and undoped TiO$_2$ (b) as function of temperature are shown in Fig. 8. Undoped sol–gel TiO$_2$ shows bands in the range 3900–900 cm^{-1} related to the presence of water, according to 1633 cm^{-1} stretching band, and to OH vibrations at 3769, 3720–24, 3731–33 cm^{-1} (isolated, bridged and vicinal groups). Low absorptions at 2850–3060 are typical of titania samples. As samples temperature increased the water desorbed and, correspondingly, the associated absorptions decreased up to disappear at 400 °C.
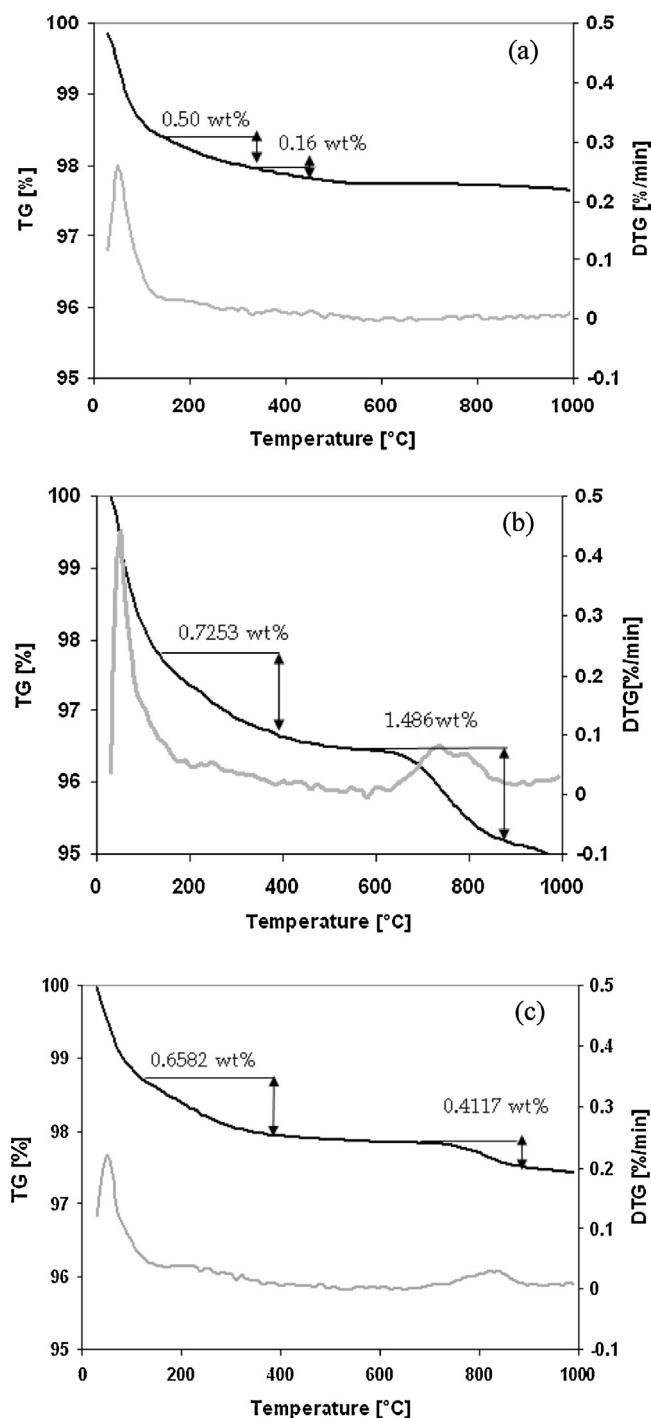
Fig. 4. TG analysis of NDT (a), PC100 (b) and PC50 (c) photocatalysts.

Fig. 5. Raman spectra of PC50, PC100 and NDT photocatalysts.
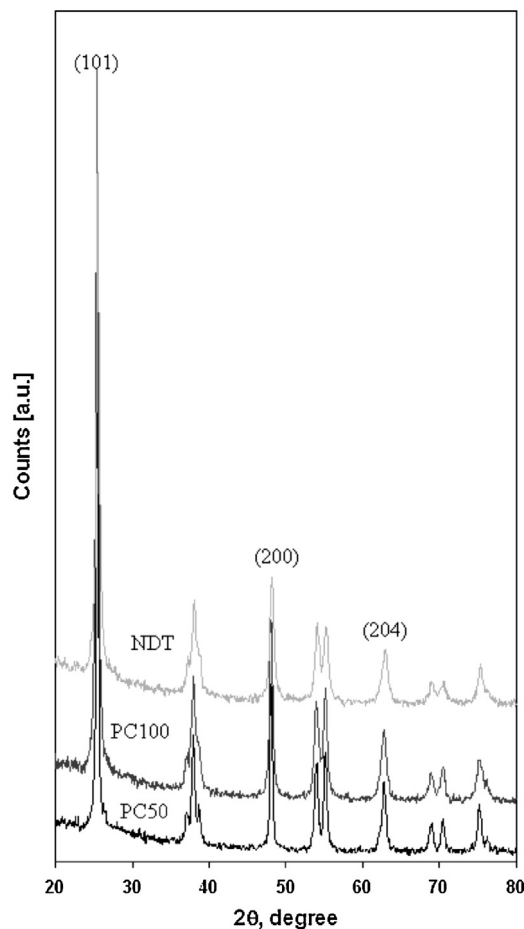
Fig. 6. XRD spectra of PC50, PC100 and NDT photocatalysts.

NDT titania show new bands at 2050–53, 2166, 2214–17, 2345 cm^{-1} and a composite peak with three maxima at 2350, 2360, 2364 cm^{-1}; these peaks can be attributed to the N atoms embedded in the TiO$_2$ network, or present in its surface. Moreover, these bands could be attributed to several N forms. At 2056 cm^{-1} a N bounded by a triple bond vibrates, and so the band at 2046 cm^{-1} could be likely due to the presence of this kind of surface specie. Peaks at 2166 and 2214–17 cm^{-1} resemble the absorptions of isocianate species bonded to Ti, such as 2M-N=C=O (2147 cm^{-1}, 2210 cm^{-1}) [33] while the composite bands around 2360 cm^{-1} are indicative of NO$^+$, whose presence was detected by a different characterization technique on N-TiO$_2$ photocatalysts. The presence of three maxima
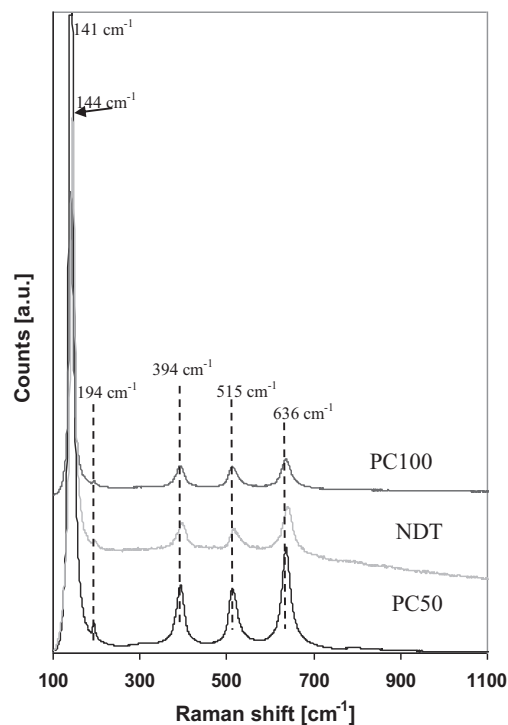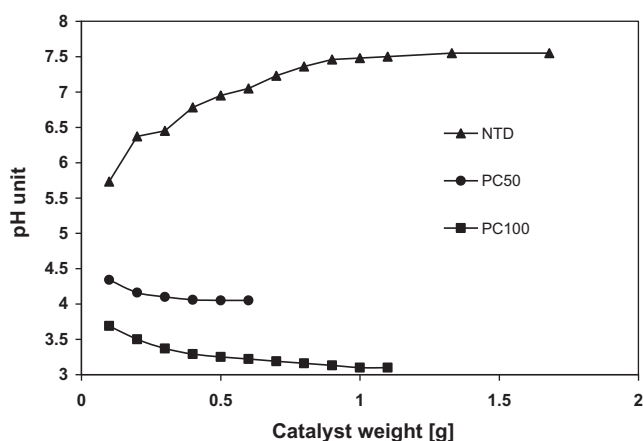
Fig. 7. PZC estimation by mass titration method: pH behavior as a function of photocatalyst powder addiction.

in the absorption band could be related to the occurring of different kind of nitrosil ions, interstistial and substitutional, as revealed by XPS measurements [34]. At higher temperature pretreatment, no significant changes with respect the main peaks was observed. The intensity of bands increases, indicating that the removal of water leads to better evidence of the typical N related absorptions. However, hydroxyls stretching frequency remains almost the same that in undoped titania, but it is worthwhile to note that they are already present at 400 °C, with a residual and relevant intensity, with the prevalence of 3688 cm^{-1} absorption. A wide band in the range 3050–3600 cm^{-1} could indicate the presence of different surface NH terminal groups. Some of these are emphasized at higher temperatures, in particular at 350 and 400 °C. From this broad signal emerges a band, around 3170 cm^{-1} assignable to NH stretching of –NH$_2$ groups, confirmed by the presence of 1467 and 1571 cm^{-1} bands. Other contributions at higher wavenumbers can be ascribed to OH groups and it must be observed that at 400 °C, NDT preserves yet its hydroxyls, in particular bridged OH, vibrating at lower frequencies (3688 cm^{-1}). In addition to the water bending at 1630 cm^{-1}, a band at 1388 cm^{-1} is found, probably due to an NO vibration.

So a more complex picture of the surface emerges from FT-IR analysis, beyond the nitrosyl groups presence, where ammino and isocianate groups (coming from the not complete removal of the precursor organic part), appear responsible for the higher basicity of NDT, with respect to the more acid undoped TiO$_2$. Further N-species are likely located as terminal groups linked to Ti, while bridged OH are already present and stabilized on the surface also at high calcination temperature.

3.1.8. Particles size analysis in aqueous phase

Weighted average size of titania aggregates is reported in Table 3 as function of TiO$_2$ concentration in aqueous phase.

For NDT aggregates, size ranges between 318 and 482 nm. For PC50 and PC100 bigger sizes were found within the ranges 928–1216 nm and 706–1204 nm, respectively. For the both latter titanias, a tendency to an increased size as titania concentration was increased can be observed.

3.2. Optimization of N-doped TiO$_2$ loading for the inactivation tests

The effect of NDT loading on E. coli strain inactivation was investigated in the range 0.025–0.5 g L^{-1} after 10 min irradiation time (Fig. 9). Although solar light or simulated solar light has a bactericidal effect, the addition of photocatalyst results in a faster

bacterial inactivation [13]; in our experiments, simulated solar radiation alone resulted in a significantly lower initial inactivation rate (1.25×10^5 CFU 100 mL^{-1} min^{-1}) compared to that observed in the presence of catalyst (Fig. 9). In particular, the higher initial inactivation rate (8.5×10^5 CFU 100 mL^{-1} min^{-1}) was observed for 0.2 g L^{-1} photocatalyst loading. The inactivation rate increases when catalyst loading increases from 0.025 to 0.2 g L^{-1} indicating that the addition of more titania particles enhanced the number of the photoactive sites in the solution. At concentrations higher than 0.2 g L^{-1}, the decrease of E. coli strain inactivation may be due to the aggregation of free TiO$_2$ particles (increased NDT particle size, Table 3) that results in a decrease in the number of surface active sites [35]. Further, the excessive opacity and screening effect due to the higher TiO$_2$ loading act as shield, and consequently hinder the light penetration. Therefore, there is loss of available surface area for light-harvesting which results in a reduction of the catalytic activity [36].

According to the scientific literature, the optimum photocatalyst loading mainly depends on the photoreactor and the light intensity [13]. For instance, 0.05 g L^{-1} of TiO$_2$ P25 was found to be the optimal catalyst concentration in the inactivation of E. coli by solar photocatalysis with compound parabolic collectors [10]; but 0.01 g L^{-1} of TiO$_2$ P25 (400 W sodium lamp located 10 cm from the reaction vessel) were enough to successfully inactivate E. coli, Pseudomonas aeruginosa, and Staphylococcus aureus, within 40 min [37]. Moreover, some studies on the E. coli inactivation with N-doped TiO$_2$ have been reported but different results were observed. Liu et al. [7] observed a high efficiency with a total inactivation (initial bacterial density 10^9 CFU mL^{-1}) after 120 min irradiation under solar light (10 mW cm^{-2}). In contrast, a comparatively poor efficiency (just 50% E. coli inactivation after 120 min irradiation, initial bacterial density 10^6 CFU mL^{-1}) was observed in a subsequent study under simulated solar light (total intensity: 550 W m^{-2}; UV intensity 20–30 W m^{-2}; concentration of TiO$_2$ powders of 1 g L^{-1}) [38].

3.3. Comparison among catalysts

NDT catalyst was found to be the most effective catalyst to inactivate the antibiotic resistant E. coli strain for all investigated catalysts loadings (Fig. 10).

The higher inactivation rate (89.47%) after 10 min of irradiation time was observed at 0.2 g L^{-1} catalyst loading. PC100 was found to be more effective than PC50 for the lower investigated catalysts loadings, but PC50 and P100 were less effective as catalyst loading was increased up to 0.5 g L^{-1}, likely due to photons transfer limitations at higher titania concentration, as previously discussed. It could be argued that the tendency to the aggregation, and consequently the size of aggregates of titania nanoparticles may influence the ability of the different titanias to inactivate bacterial colonies. The size of the aggregates is dependent mainly on the specific surface area of titania, surface characteristics and concentration [39]. Accordingly, the decreasing trend in the inactivation ability observed at higher concentration could be also related to an increased TiO$_2$ aggregates size in the solution. Fig. 10 also depicts the values of the particle size. In the case of PC100 there is a fairly agreement among the changing of aggregate size and the variation of inactivation percentage. The higher activity of PC50 may be due to the lower aggregates size for photocatalyst loading less than 0.3 g L^{-1}. For higher titania loading, the inactivation percentage is similar for PC50 and PC100. Surprisingly, the average aggregate size is similar for both titania showing that the larger aggregates play a negative effect on the inactivation. Accordingly, the decrease in the percentage of inactivated E. coli for NDT is not significant, and this result is in agreement with the presence of aggregates of lower size whose dimensions did not change significantly as catalyst loading was changed (Fig. 10). pH was also measured during comparison
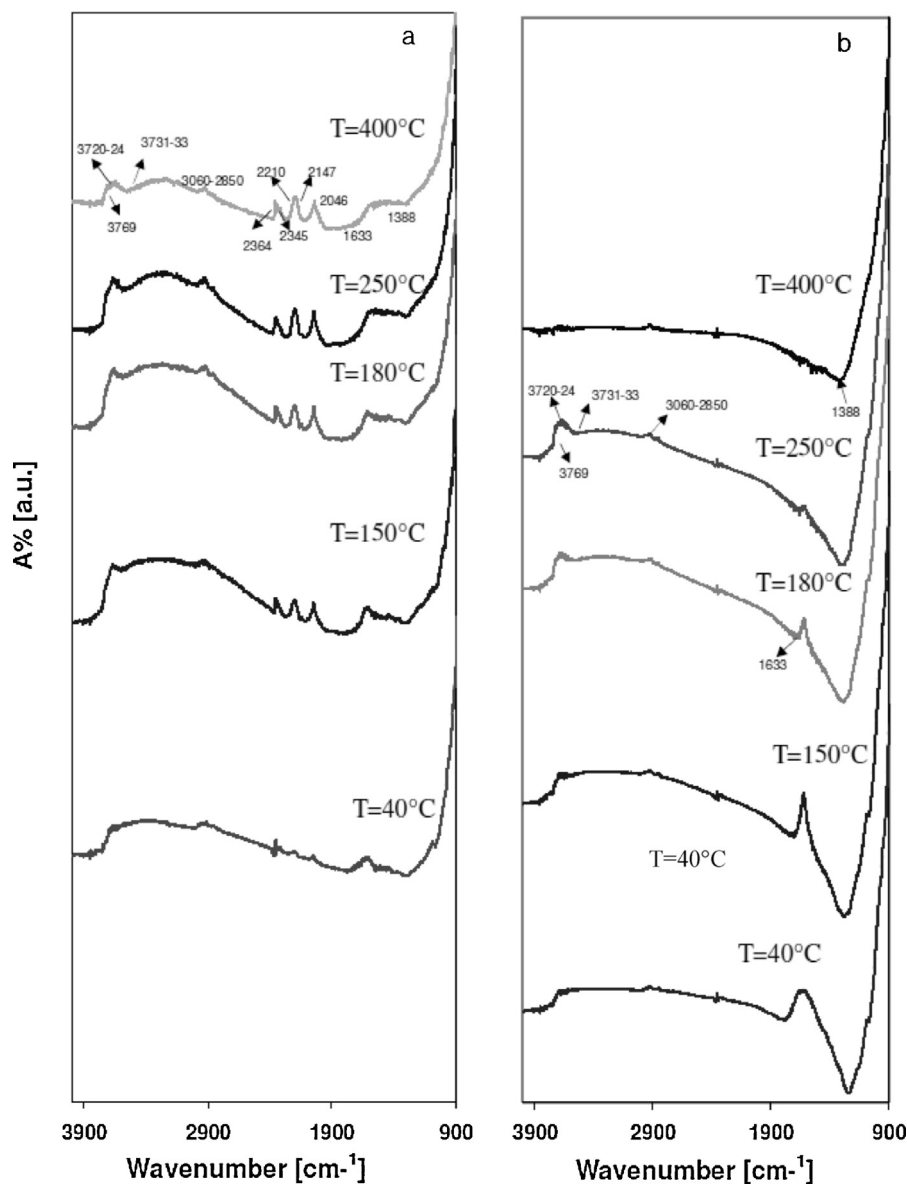
Fig. 8. FTIR spectra analysis of NDT (a) and undoped TiO_2 (b) as function of temperature.

tests and it was found to vary in the range 4.4–5.4. But pH did not affect inactivation efficiency (data not shown). This result can be explained according to PZC data (Fig. 7) because the pH variation during photocatalytic tests did not result in any charge inversion in the suspension.

3.4. Inactivation kinetic

The optimum photocatalyst loading ($0.2\,g\,L^{-1}$) for NDT was used to investigate the inactivation kinetic of antibiotic resistant *E. coli* strain. As it can be observed from Fig. 11, a total inactivation took place within 60 min irradiation.

Table 3
Aggregates size of PC50, PC100 and NDT photocatalysts.

Catalyst loading ($g\,L^{-1}$)	PC50 size (nm)	PC100 size (nm)	NDT size (nm)
0.1	947	706	356
0.2	928	799	319
0.3	1216	1204	482
0.5	1108	1025	318

Typically, disinfection efficiency of photocatalytic process has been investigated using pure culture of microorganisms (mainly *E. coli*) suspended in purified or deionized water [10,13,15]. On the opposite, only a few studies addressed real wastewater and
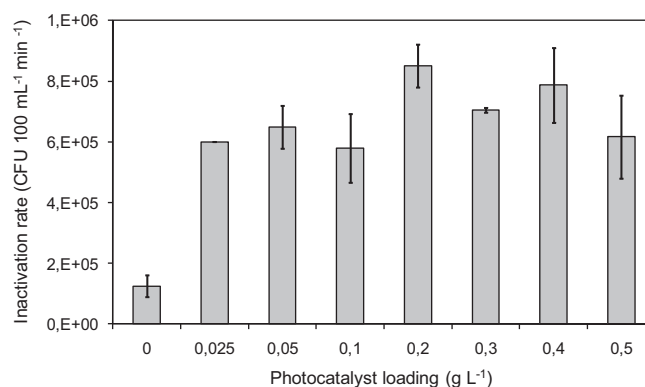

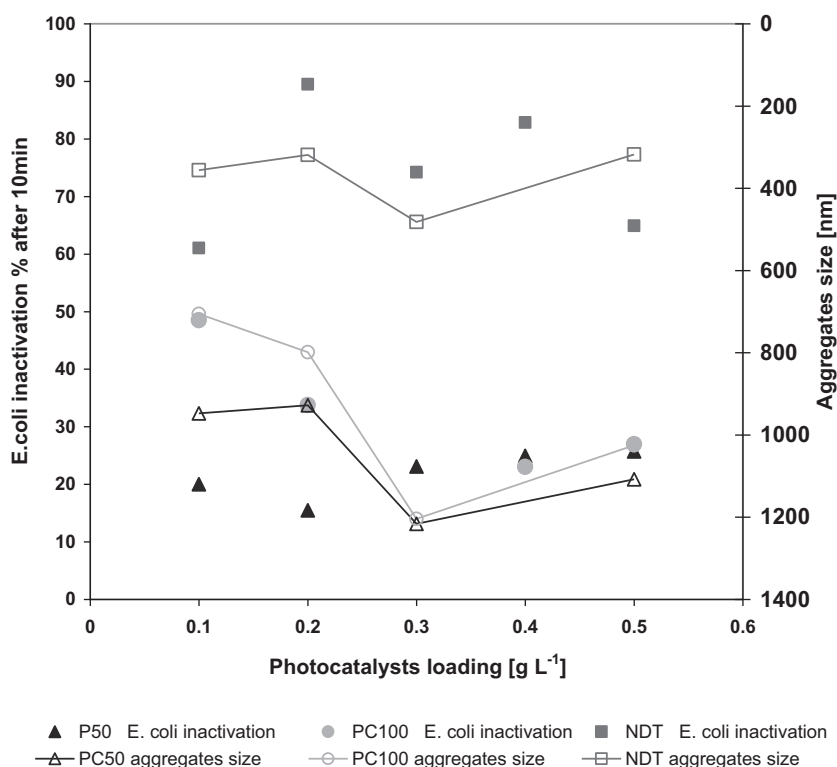**Fig. 9.** Initial inactivation rate as a function of NDT loading.

Fig. 10. *E. coli* inactivation and aggregates size as a function of photocatalysts loading.

natural bacteria [40]. To our knowledge, this is the first work where the effect of photocatalytic process was investigated in the inactivation of a natural *E. coli* antibiotic resistant strain in real wastewater. The inactivation kinetic achieved in our work is comparable with the results observed in previous works with deionized water *E. coli* suspensions. Liu et al. [7] observed a total inactivation (10^9 CFU mL^{-1} initial *E. coli* density) within 120 min of irradiation (average light intensity 10 mW cm^{-2}), using an N-doped TiO$_2$ photocatalyst. Moreover, Rengifo-Herrera et al. [12] achieved an *E. coli* inactivation rate (10^4 CFU mL^{-1} initial *E. coli* density) higher in N, S doped TiO$_2$ nanoparticles (total inactivation in approximately 80 min) than in pure TiO$_2$ powders (no total inactivation was observed also after 120 min treatment), under visible light irradiation (average light intensity in the range 290–1100 nm: 6 mW cm^{-2}).
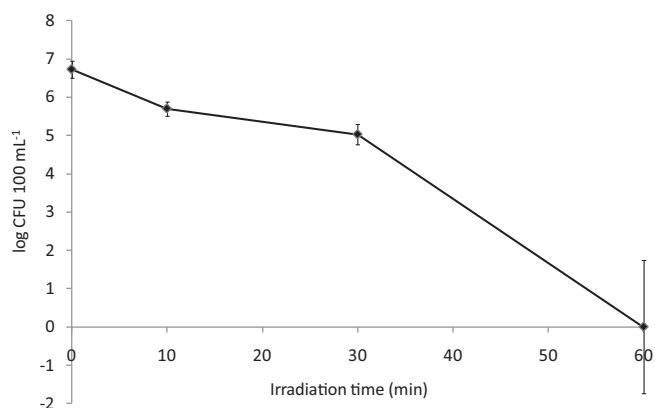
3.5. Effect of photocatalytic process on antibiotic resistance

Fig. 12 shows the results of antibiotic resistance of *E. coli* strain to the target antibiotics investigated (CIP, CEF, TET and VAN) according to Kirby–Bauer test. When bacterial colonies grow, a ring which marks the inhibition capacity of the antibiotic on the bacterial growth can be observed around the antibiotic disk. The larger the inhibition diameter of antibiotic disk, the lower the bacterial resistance to the antibiotic.

The average value of inhibition diameter for CIP before photocatalytic treatment ($t = 0$) was 12.5 mm. Compared to the corresponding clinical breakpoints values for *E. coli*, from EUCAST database [41] (susceptible (S) $\geq$ 22 mm; 22 < intermediary (I) $\leq$ 19 mm; resistant (R) < 19 mm), the *E. coli* strain used in this work was found to be resistant to CIP. Moreover, solar photocatalytic process with NDT affected its resistance to some extent,
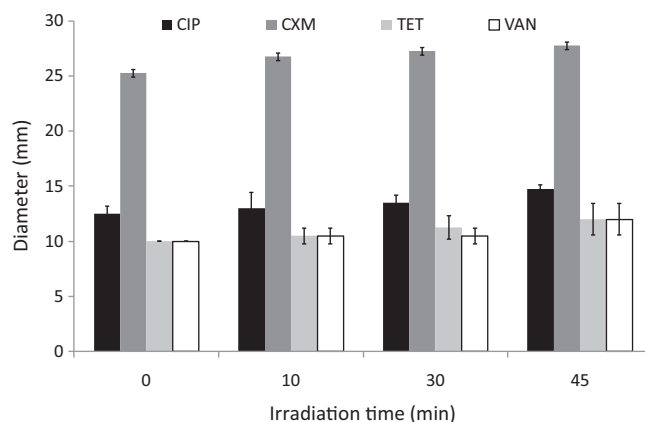

Fig. 11. Inactivation kinetic of antibiotic resistant *E. coli* strain as a function of irradiation rime with NDT photocatalyst.

Fig. 12. Antibiotic resistance of *E. coli* strain to the target antibiotics investigated (CIP, CEF, TET and VAN) according to Kirby–Bauer test.

because a decreasing trend ($p < \alpha = 0.05$; $p = 0.0311$) as irradiation time increased can be observed (Fig. 12). The average value of inhibition diameter for CEF before photocatalytic treatment ($t = 0$) was 25.3 mm. Compared to the corresponding clinical breakpoints values for *E. coli* from EUCAST database ($S \geq 18$ mm; $R < 18$ mm), the *E. coli* strain is susceptible to CEF, and photocatalytic treatment affected its sensitivity to some extent, because a decreasing trend ($p < \alpha = 0.05$; $p = 0.0018$), as irradiation time increased, was observed (Fig. 12). The average value of inhibition diameter for TET and VAN before photocatalytic treatment ($t = 0$) is the same (10 mm), but unfortunately no data are available in EUCAST database for comparison. However, solar photocatalytic treatment with NDT did not significantly affect resistance of *E. coli* strain to both antibiotics as irradiation time increased.

4. Conclusion

In this work a purposely synthesized N-doped TiO$_2$ photocatalyst was investigated for the first time in the inactivation of an antibiotic resistant *E. coli* strain selected from real wastewater. N-doping by sol–gel method effectively shifted TiO$_2$ band-gap energy from 3.3–3.4 eV to 2.5 eV, thus making more effective photocatalytic disinfection process under solar radiation. In particular, a higher photocatalytic inactivation efficiency of an antibiotic resistant *E. coli* strain in a biologically treated wastewater was observed for the NDT photocatalyst compared to commercially available TiO$_2$ powders (Millennium PC50 and PC100). Kinetic test at the optimum photocatalyst loading showed that total inactivation can be achieved within 60 min of irradiation. Moreover, solar photocatalytic process with NDT did not significantly affect resistance of *E. coli* strain to TET and VAN as irradiation time increased, but a decreasing trend ($p < \alpha = 0.05$) in resistance to CIP ($p = 0.0311$) and sensitivity to CEF ($p = 0.0018$) was observed. Accordingly, a total inactivation of antibiotic resistant bacteria should be achieved to minimize the risk of antibiotic resistance spread into the receiving water. Solar photocatalytic treatment may be successfully used for the disinfection of biologically treated wastewater from small UWWTPs to produce safe water for disposal or reuse in crop irrigation.

References

[1] T. Schwartz, W. Kohnen, B. Jansen, U. Obst, FEMS Microbiology Ecology 43 (2003) 325–335.
[2] I. Michael, L. Rizzo, C.S. McArdell, C.M. Manaia, C. Merlin, T. Schwartz, C. Dagot, D. Fatta-Kassinos, Water Research 47 (2013) 957–995.
[3] L. Rizzo, C. Manaia, C. Merlin, T. Schwartz, C. Dagot, M.C. Ploy, I. Michael, D. Fatta-Kassinos, Science of the Total Environment 447 (2013) 345–360.
[4] M. Munir, K. Wong, I. Xagoraraki, Water Research 45 (2011) 681–693.
[5] L. Rizzo, Water Research 45 (2011) 4311–4340.
[6] O. Sacco, M. Stoller, V. Vaiano, P. Ciambelli, A. Chianese, D. Sannino, International Journal of Photoenergy (2012), http://dx.doi.org/10.1155/2012/626759, Article ID: 626759.
[7] Y. Liu, J. Li, X. Qiu, C. Burda, Water Science and Technology 54 (2006) 47–54.
[8] D.M.A. Alrousan, M.I. Polo-López, P.S.M. Dunlop, P. Fernández-Ibáñez, J.A. Byrne, Applied Catalysis B: Environmental 128 (2012) 126–134.
[9] U. Von Gunten, Water Research 37 (2003) 1469–1487.
[10] P. Fernandez, J. Blanco, C. Sichel, S. Malato, Catalysis Today 101 (2005) 345–352.
[11] L. Rizzo, Journal of Hazardous Materials 165 (2009) 48–51.
[12] S.D. Richardson, A.D. Thruston, T.W. Collette, K.S. Patterson, B.W. Lykins, J.C. Ireland, Environmental Science & Technology 30 (1996) 3327–3334.
[13] S. Malato, P. Fernandez-Ibanez, M.I. Maldonado, J. Blanco, W. Gernjak, Catalysis Today 147 (2009) 1–59.
[14] M. Gratzel, Nature 414 (2001) 338–344.
[15] J.A. Rengifo-Herrera, J. Kiwi, C. Pulgarin, Journal of Photochemistry and Photobiology A: Chemistry 205 (2009) 109–115.
[16] J.A. Rengifo-Herrera, K. Pierzchała, A. Sienkiewicz, L. Forró, J. Kiwi, C. Pulgarin, Applied Catalysis B: Environmental 88 (2009) 398–406.
[17] J.A. Rengifo-Herrera, K. Pierzchała, A. Sienkiewicz, L. Forró, J. Kiwi, J.E. Moser, C. Pulgarin, Journal of Physical Chemistry C 114 (2010) 2717–2723.
[18] U. Diebold, Applied Physics A: Materials Science and Processing 76 (2003) 681–687.
[19] S. Qourzal, A. Assabbane, Y. Ait-Ichou, Journal of Photochemistry and Photobiology A: Chemistry 163 (2004) 317–321.
[20] D. Sannino, V. Vaiano, O. Sacco, P. Ciambelli, Journal of Environmental Chemical Engineering 1 (2013) 56–60.
[21] J.S. Noh, J.A. Schwarz, Journal of Colloid and Interface Science 130 (1989) 157–164.
[22] L. Rizzo, A. Fiorentino, A. Anselmo, Chemosphere 92 (2013) 171–176.
[23] H. Ozaki, N. Fujimoto, S. Iwamoto, M. Inoue, Applied Catalysis B: Environmental 70 (2007) 431–436.
[24] D. Sannino, V. Vaiano, P. Ciambelli, J.J. Murcia, M.C. Hidalgo, J.A. Navío, Journal of Advanced Oxidation Technologies 16 (2013) 71–82.
[25] J.J. Murcia, M.C. Hidalgo, J.A. Navío, V. Vaiano, P. Ciambelli, D. Sannino, Catalysis Today 196 (2012) 101–109.
[26] D. Sannino, V. Vaiano, P. Ciambelli, P. Eloy, E.M. Gaigneaux, Applied Catalysis A: General 394 (2011) 71–78.
[27] T. Ihara, M. Miyoshi, Y. Iriyama, O. Matsumoto, S. Sugihara, Applied Catalysis B: Environmental 42 (2003) 403–409.
[28] J.C. Parker, R.W. Siegel, Journal of Materials Research 5 (1990) 1246–1252.
[29] M.S.P. Francisco, V.R. Mastelaro, Chemistry of Materials 14 (2002) 2514–2518.
[30] D. Sannino, V. Vaiano, P. Ciambelli, Catalysis Today 205 (2013) 159–167.
[31] P. Ciambelli, D. Sannino, V. Palma, V. Vaiano, Studies in Surface Science and Catalysis 155 (2005) 179–187.
[32] A. Sorrentino, S. Rega, D. Sannino, A. Magliano, P. Ciambelli, E. Santacesaria, Applied Catalysis A: General 209 (2001) 45–57.
[33] R.J.H. Clark, Applied Organometallic Chemistry 13 (1999) 858.
[34] C. Di Valentin, E. Finazzi, G. Pacchioni, A. Selloni, S. Livraghi, M.C. Paganini, E. Giamello, Chemical Physics 339 (2007) 44–56.
[35] C.C. Chen, C.S. Lu, Y.C. Chung, J.L. Jan, Journal of Hazardous Materials 141 (2007) 520–528.
[36] J. Lea, A.A. Adesina, Journal of Photochemistry and Photobiology A: Chemistry 118 (1998) 111–122.
[37] O. Seven, B. Dindar, S. Aydemir, D. Metin, M.A. Ozinel, S. Icli, Journal of Photochemistry and Photobiology A: Chemistry 165 (2004) 103–107.
[38] J.A. Rengifo-Herrera, C. Pulgarin, Solar Energy 84 (2010) 37–43.
[39] D. Jassby, J. Farner Budarz, M. Wiesner, Environmental Science and Technology 46 (2012) 6934–6941.
[40] N. Lydakis-Simantiris, D. Riga, E. Katsivela, D. Mantzavinos, N.P. Xekoukoulotakis, Desalination 250 (2010) 351–355.
[41] EUCAST, European Committee on Antimicrobial Susceptibility Testing, http://www.eucast.org/